

Vertex dynamics simulations of viscosity-dependent deformation during tissue morphogenesis

Satoru Okuda · Yasuhiro Inoue · Mototsugu Eiraku ·
Taiji Adachi · Yoshiki Sasai

Received: 11 May 2014 / Accepted: 26 August 2014 / Published online: 17 September 2014
© Springer-Verlag Berlin Heidelberg 2014

Abstract In biological development, multiple cells cooperate to form tissue morphologies based on their mechanical interactions; namely active force generation and passive viscoelastic response. In particular, the dynamic processes of tissue deformations are governed by the viscous properties of the tissues. These properties are spatially inhomogeneous because they depend on the tissue constituents, such as cytoplasm, cytoskeleton, basement membrane and extracellular matrix. The multicellular mechanics of tissue morphogenesis have been investigated in vertex dynamics models. However, conventional models are applicable only to quasi-static deformation processes, which do not account for tissue viscosities. We propose a vertex dynamics model that simulates the viscosity-dependent dynamic deformation processes during tissue morphogenesis. By incorporating local velocity fields into the governing equation of vertex movements, the model

turns Galilean invariant. In addition, the viscous properties of tissue components are newly expressed by formulating friction forces on vertices as functions of the relative velocities among the vertices. The advantages of the proposed model are examined by epithelial growth simulations under the employed condition for quasi-static processes. As a result, the epithelial vesicle simulated by the proposed model is linearly elongated with nearly free stress, while that simulated by the conventional model is undulated with compressive residual stress. Therefore, the proposed model is able to reflect the timescale of deformations by satisfying Galilean invariance. Next, the applicability of the proposed model is assessed in epithelial growth simulations of viscous extracellular materials. In this test, the epithelial vesicles are deformed into tubular shapes by oriented cell divisions, and their morphologies are extremely sensitive to extracellular viscosity. Therefore, the dynamic deformations in the proposed model depend on the viscous properties of tissue components. The proposed model will be useful for simulating dynamic deformation processes of tissue morphogenesis depending on viscous properties of various tissue components.

Electronic supplementary material The online version of this article (doi:[10.1007/s10237-014-0613-5](https://doi.org/10.1007/s10237-014-0613-5)) contains supplementary material, which is available to authorized users.

We dedicate this article to the memory of Dr. Yoshiki Sasai, who suddenly passed away on August 5, 2014 at the beginning of our project exploring mechanics in developmental morphogenesis.

S. Okuda (✉) · Y. Sasai
Organogenesis and Neurogenesis Group,
Center for Developmental Biology, RIKEN,
2-2-3 Minatojima-Minamimachi, Chuo-ku, Kobe,
Hyogo 650-0047, Japan
e-mail: okuda@cdb.riken.jp

Y. Inoue · T. Adachi
Department of Biomechanics, Institute for Frontier Medical Sciences, Kyoto University, Kyoto, Japan

M. Eiraku
Four-Dimensional Tissue Analysis Unit, Center for Developmental Biology, RIKEN, Kobe, Japan

Keywords Multicellular morphogenesis · Dynamic deformation process · Viscous property · Vertex dynamics model · Computational biomechanics · Developmental biomechanics

1 Introduction

Tissue morphogenesis is accompanied by characteristic deformations in three-dimensional (3D) space, such as epithelial invagination (Letizia et al. 2011), evagination (Eiraku et al. 2011), elongation (Heisenberg et al. 2000; Davies 2005), torsion (Taniguchi et al. 2011) and branching

(Metzger et al. 2008). Mechanical forces driving these tissue deformations are actively generated during characteristic cellular activities such as contraction, adhesion, migration and proliferation (Lecuit and Lenne 2007; Rauzi et al. 2010; Woolner and Papalopulu 2012; Rauzi et al. 2008). Concomitantly, cells passively respond to these forces in a viscoelastic manner (Park et al. 2005; Unterberger et al. 2013). Such cellular mechanical interactions are spatiotemporally orchestrated on multicellular scales. Hence, to reveal the mechanics of tissue morphogenesis, we must understand the relationship between active force generation and passive viscoelastic response at the multicellular level.

The viscous properties of tissues play an important role in passive response, because they govern the dynamic processes of tissue deformations. According to a recent study of Drosophila gastrulation, cytoplasmic displacements can be temporally described by hydrodynamic viscous flows in the tissue (Doubrovinski et al. 2014). This suggests that tissue deformation arises from the viscous response of the cytoplasm. Moreover, the viscous properties of tissues are probably spatially inhomogeneous because they should depend on tissue components, such as cytoplasm, cytoskeleton, basement membrane and extracellular matrix. For instance, the fusion of two cell aggregates can be explained by balance between the tissue surface tension and an opposing effective viscous property of the tissue (Borghi and James 2009). The estimated viscous property of cell aggregates (10^4 – 10^7 Pas) far exceeds those of water (10^{-3} Pas) and cytoplasm (10^2 Pas), possibly reflecting dissipative processes in cell rearrangements occurring through intercellular bond rupture (Brochard-Wyart and de Gennes 2003), cytoskeletal relaxation or remodeling (Cuvelier et al. 2007) or membrane recycling. Crucially, these viscosity-dependent deformations can be regulated by the timing of cellular cues that generate active forces, which are likely to complicate the mechanics of tissue deformations. Thus, to understand the mechanics in tissue morphogenesis, investigating viscosity-dependent dynamic deformation processes during tissue morphogenesis would be valuable.

Multicellular morphodynamics have been analyzed by vertex dynamics models (Odell et al. 1981; Honda et al. 1984, 2004). These models reproduce the multicellular dynamics of several cellular mechanical behaviors. For example, cell rearrangement—a necessary process in plastic tissue deformations—is modeled by reconnecting a vertex network (Honda et al. 1984, 2004; Okuda et al. 2013a). Moreover, cell division—a process in rapid tissue growth—is replicated by dividing a cellular element in the network (Honda et al. 1984; Okuda et al. 2013b). Therefore, vertex dynamics models are eminently suitable for modeling tissue processes and have been successfully applied to elastic–plastic deformations in various morphological phenomena, including geometrical pattern formations of epithelial cells (Farhadifar et al.

2007; Dahmann et al. 2011), convergent–extension processes (Honda et al. 2008) and epithelial evagination (Osterfield et al. 2013).

Conventional vertex dynamics models describe vertex dynamics by minimizing a potential energy using a Monte Carlo method or an overdamped equation of motion in a quasi-static state. Hence, conventional models are applicable only to quasi-static deformation processes and cannot account for tissue viscosities. By incorporating local viscous friction and local velocity vectors into a 2D vertex model, the tissue's viscous properties have been successfully taken into account (Mao et al. 2013). In this model, the tissue's viscous properties are simply expressed as parameters that are weighted by global and local vertex velocities. Further, to express viscous effects of each tissue component depending on its geometry, we require a new framework that relates the geometry and viscosity of each tissue component to the vertex dynamics.

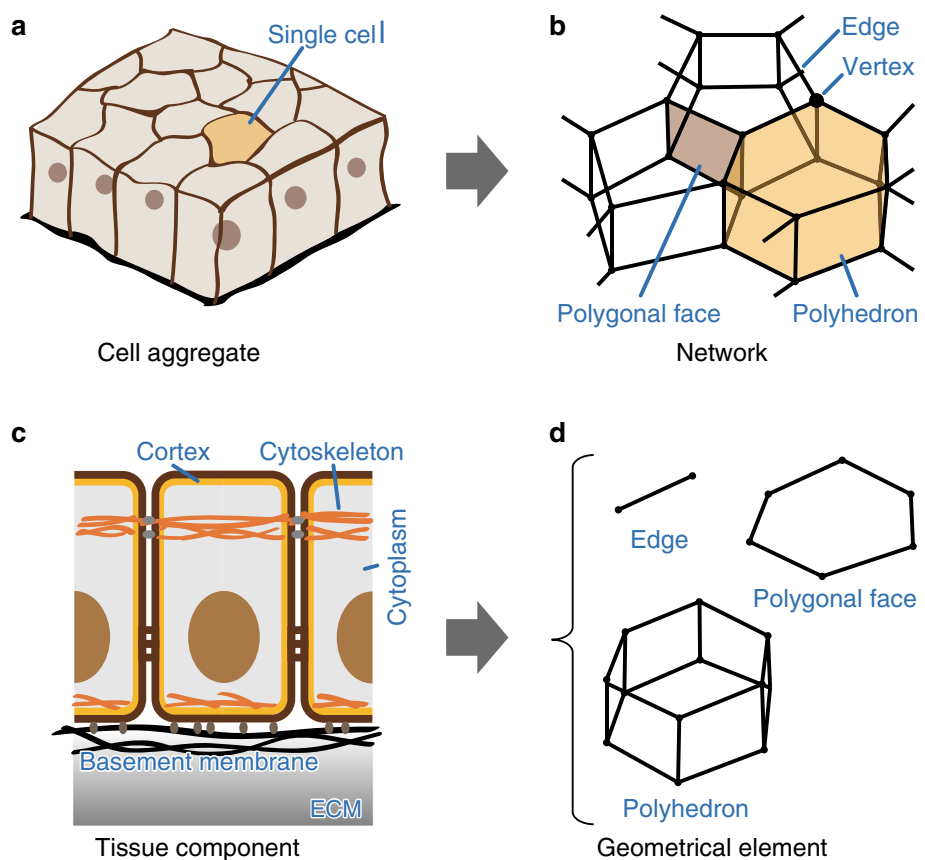
The overdamped equation used in conventional models involves a term of viscous friction force, which is assumed to linearly vary with the vertex velocity in the global coordinate system. Thus, if the conventional models were applied to dynamic deformation processes, global tissue deformations would create viscous resistance forces. This is because vertex dynamics in conventional models are variant under the coordinate transformation, which is referred to as the violation of Galilean invariance (Goldstein et al. 2001). Therefore, to simulate dynamic tissue deformations by vertex dynamics models, we require that the vertex dynamics satisfy the Galilean invariance.

The present study proposes a vertex dynamics model for simulating viscosity-dependent dynamic deformation processes during tissue morphogenesis. Local velocity vectors are introduced into the governing equation of vertex movements. In addition, the model accounts for the viscous properties of tissue components by formulating the viscous friction force on vertices as functions of the relative velocities among the vertices. The advantage and applicability of the proposed model is evaluated in the simulated morphodynamics of a directional epithelial growth surrounded by viscous extracellular materials. Based on the results, we discuss the morphological dependence on extracellular viscosity from a biomechanical viewpoint.

2 Formulating viscosity-dependent dynamic deformation process in a vertex dynamics model framework

Three-dimensional vertex dynamics models (Honda et al. 2004; Okuda et al. 2013a) represent single cells by polyhedra, as shown in Fig. 1a, b. The polygonal faces are shared by neighboring polyhedra, and the vertices and edges com-

Fig. 1 Expressing tissue components in the proposed vertex dynamics model. **a** Illustration of multicellular tissue. **b** Illustration of network composed of vertices and edges. Each single cell (yellow in **a**) is modeled by a single polyhedron (yellow in **b**), and neighboring polyhedrons share the polygonal faces of their boundaries (brown in **b**). **c** Schematic diagram of tissue components such as cytoplasm, cytoskeleton, cellular cortex, basement membrane and ECM. **d** Diagram of geometrical elements (edge, polygonal face and cellular polyhedron)



prise a single network that represents the entire shape of a cell aggregate. Within this network, each vertex is connected to four edges. A polygonal face with four or more edges is described by radially arranged triangles composed of each edge and the center point of the polygonal face (Okuda et al. 2013a). To express cell rearrangements, local network patterns are reconnected using the reversible network reconnection (RNR) model (Okuda et al. 2013a). Hence, the dimensions of cellular polyhedra and facial polygons are variable depending on cell shapes and configuration. For instance, in a monolayer cell sheet with homogeneous cell properties, cellular polyhedra typically have the geometry of a hexagonal column composed of eight facial polygons.

In the proposed model, the multicellular dynamics are expressed by vertex movements derived from local velocity fields (Mao et al. 2013; Ishimoto et al. submitted). The movement of the i^v th vertex at position \mathbf{r}_{i^v} is given by

$$\eta_{i^v}^v \left(\frac{d\mathbf{r}_{i^v}}{dt} - \mathbf{v}_{i^v}^f \right) = -\nabla_{i^v} U. \quad (1)$$

The left-hand side of Eq. (1) is the viscous friction force exerted on the i^v th vertex, whose scalar $\eta_{i^v}^v$ is the viscous friction coefficient of that vertex. Vector $\mathbf{v}_{i^v}^f$ denotes the local velocity vector around the i^v th vertex, which is newly defined as a function of the velocity vectors at vertices. The right-hand side of Eq. (1) is the conservative force acting on the

i^v th vertex, where ∇_{i^v} is the gradient at the i^v th vertex position, and U is a potential energy embodying the energetic properties and behaviors of tissue.

Multicellular tissue comprises various components such as cytoplasm, cytoskeleton, cellular cortex, basement membrane and extracellular matrices (ECM). In the proposed model, the viscous properties of these components are expressed by friction among the vertices of each geometrical element in the network (edge, polygonal face and cellular polyhedron), as shown in Fig. 1c, d.

The viscous friction coefficient $\eta_{i^v}^v$ in Eq. (1) is simply defined as follows

$$\eta_{i^v}^v = \sum_{j^e}^{\text{element}} \eta_{j^e}^e \delta_{i^v, j^e}, \quad (2)$$

where $\sum_{j^e}^{\text{element}}$ is the summation over all geometrical elements. The binary function δ_{i^v, j^e} is 1 if the j^e th geometrical element contains the i^v th vertex and 0 otherwise. The constant $\eta_{j^e}^e$ is the viscous friction weight of vertices in the j^e th geometrical element.

To balance the total viscous friction force within each geometrical element, the local velocity vector around the i^v th vertex $\mathbf{v}_{i^v}^f$ in Eq. (1) is defined as the mean velocity vector of the surrounding geometrical elements:

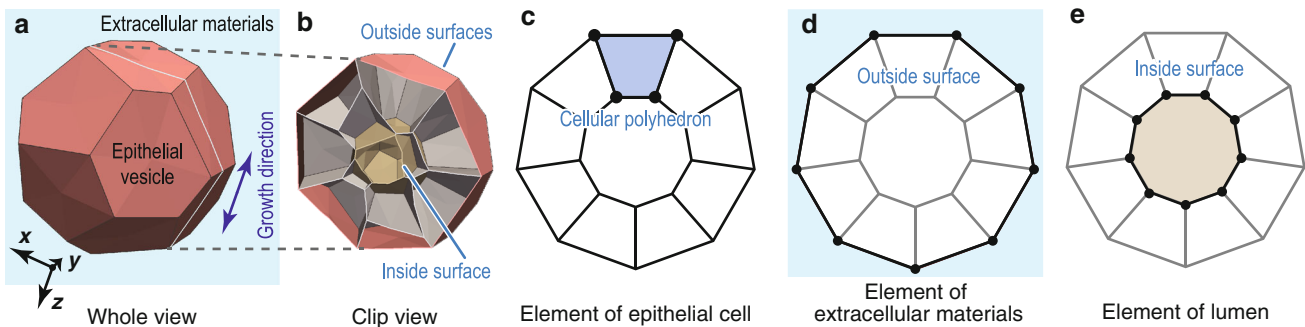


Fig. 2 Initial structure of an epithelial vesicle surrounded by extracellular materials. **a** Whole view of tissue under the initial condition. The epithelial vesicle (orange polyhedron) comprising 18 cells is surrounded by viscous extracellular materials (light blue area). The epithelial vesicle grows by cell divisions oriented in the growth direction. **b** Clipped view of tissue. The epithelial vesicle has a monolayer sheet structure with an interior surface (brown area) and outside surface (red area). **c** Cross section of a geometrical element expressing an epithelial

cell (dark blue area). The geometrical element of each cell is a set of vertices forming a single cellular polyhedron. **d** Cross section of a geometrical element expressing viscous extracellular materials (light blue area). The geometrical element of viscous extracellular materials is a set of vertices delineating the outside surface of the epithelial vesicle. **e** Cross section of a geometrical element expressing lumen (gray area). The geometrical element of the lumen is a set of vertices delineating the interior surface of the epithelial vesicle

$$\mathbf{v}_{iv}^f = \frac{\sum_{j^e}^{\text{element}} \eta_{j^e}^e \mathbf{v}_{j^e}^e \delta_{iv; j^e}}{\sum_{j^e}^{\text{element}} \eta_{j^e}^e \delta_{iv; j^e}}. \quad (3)$$

In Eq. (3), the vector $\mathbf{v}_{j^e}^e$ is the velocity of the j^e th geometrical element as follows:

$$\mathbf{v}_{j^e}^e = \frac{1}{n_{j^e}^e + n_{j^e}^{\text{ext}}} \left(\sum_{k^v}^{\text{vertex}} \frac{d\mathbf{r}_{kv}}{dt} \delta_{kv; j^e} + n_{j^e}^{\text{ext}} \mathbf{v}_{j^e}^{\text{ext}} \right), \quad (4)$$

where $n_{j^e}^e$ is the number of vertices comprising the j^e th geometrical element, and $\sum_{k^v}^{\text{vertex}}$ denotes summation over all vertices. The vector $\mathbf{v}_{j^e}^{\text{ext}}$ is the velocity of extracellular materials in the j^e th geometrical element, and $n_{j^e}^{\text{ext}}$ weighs the extracellular materials. In the absence of extracellular viscosity ($n_{j^e}^{\text{ext}} = 0$), the viscous friction forces at the vertices of each geometrical element are balanced (see “Balance of friction forces among the vertices of a geometrical element” section of “Appendix”). The Galilean invariance of the proposed vertex dynamics model was evaluated and confirmed in theoretical analyses (see “Galilean invariance of vertex dynamics model” section of “Appendix”). In contrast, the conventional models without local velocity vectors (Honda et al. 2004; Okuda et al. 2013a,b,c) were found to violate the Galilean invariance. Consequently, global tissue deformations could generate viscous resistance in these models. The proposed model overcomes this problem by including the local velocity vectors.

3 Computational simulations of directional epithelial growth surrounded by viscous extracellular materials

The advantage and applicability of the proposed model was evaluated in morphodynamics simulations of epithelial

growth. In general, the bodies of multicellular organisms comprise several layers of epithelial sheets. The spaces between these layers are filled by extracellular materials, such as the extracellular matrix, lumen and liquids. In particular, the extracellular matrix is a gel composed of fibrous proteins, which can be passively deformed by extrinsic forces. However, their mechanical effects on epithelial morphogenesis have as yet been little understood. Hence, to focus on the effects of their viscosity on tissue morphogenesis, in this study, we simply suppose directional tissue growth in stationary extracellular materials. This supposition also corresponds to the experimental condition for the 3D cultures of tissues covered by gel. As a simple example, the initial morphology of the epithelium is supposed to be a spherical vesicle enclosed by a monolayer cell sheet, and the vesicle is supposed to be composed of 18 proliferative cells, as shown in Fig. 2a, b. In addition, the system space is supposed to be occupied by three components: epithelial cells, extracellular materials and lumen. The space within polyhedra comprising the vesicle comprises epithelial cells, as shown in Fig. 2c. The space surrounding the epithelial vesicle comprises viscous extracellular materials, as shown in Fig. 2d. The space surrounded by the epithelial vesicle comprises a lumen, as shown in Fig. 2e, which is supposed to be passively deformed without generating any resistance force.

3.1 Expressing the mechanical properties and behaviors of tissues

To simplify the simulations, the mechanical properties and behaviors of tissues are simply expressed. The tissue components are modeled by three compartments (cells, extracellular materials and lumen), as shown in Fig. 2c–e, respectively. In the proposed model, a geometrical element of the i^c th cell is

defined as a set of vertices delineating the i^c th cellular polyhedron. A geometrical element of the extracellular materials is defined as a set of vertices delineating the outside surface of the epithelial vesicle. A geometrical element of the lumen is defined as a set of vertices delineating the interior surface of the epithelial vesicle.

The viscous friction weight in each geometrical element $\eta_{j^e}^e$ is given by

$$\eta_{j^e}^e = \begin{cases} \eta_0^{ce} & \text{epithelial cells} \\ \eta_0^{ee} & \text{extracellular materials} \\ 0 & \text{lumen,} \end{cases} \quad (5)$$

where the constants η_0^{ce} and η_0^{ee} denote the viscous friction weights of cells and extracellular materials, respectively.

From Eq. (4), the velocity of the j^e th geometrical element $v_{j^e}^e$ is written as

$$v_{j^e}^e = \begin{cases} \frac{1}{n_{j^e}^e} \sum_{k^v}^{\text{vertex}} \frac{d\mathbf{r}_{k^v}}{dt} \delta_{k^v, j^e} & \text{epithelial cells} \\ \mathbf{0} & \text{extracellular materials} \\ \mathbf{0} & \text{lumen,} \end{cases} \quad (6)$$

where $\sum_{k^v}^{\text{vertex}}$ sums overall vertices of the j^e th cellular polyhedron. Here, the extracellular materials are assumed stationary ($\mathbf{v}_{j^e}^{\text{ext}} = \mathbf{0}$), and a no-slip boundary condition is imposed between the epithelial cells and the extracellular materials ($n_{j^e}^{\text{ext}} = \infty$).

To demonstrate the advantage of the proposed vertex dynamics model, the potential energy U in Eq. (1), expressing the energetic properties and behaviors of tissue, is assigned the simple form

$$U = \sum_{i^c}^{\text{cell}} u_{i^c}^{\text{cv}} + \sum_{i^c}^{\text{cell}} u_{i^c}^{\text{cs}}, \quad (7)$$

where $u_{i^c}^{\text{cv}}$ and $u_{i^c}^{\text{cs}}$ represent potential energy functions of the osmotic energy and surface energy of the i^c th epithelial cell, respectively.

The potential energy function of the osmotic energy $u_{i^c}^{\text{cv}}$ of the i^c th cell is given by

$$u_{i^c}^{\text{cv}} = -n_{i^c}^{\text{cm}} k_B T \log \left(\frac{v_{i^c}^{\text{cv}}}{v_0^{\text{cv}}} \right), \quad (8)$$

where the constant $n_{i^c}^{\text{cm}}$ is the number of molecules in the i^c th cell, and $k_B T$ is the unit energy. To express cell growth, the variable $n_{i^c}^{\text{cm}}$ is randomly increased from $(2/3)n_0^{\text{cm}}$ to $(4/3)n_0^{\text{cm}}$ within the time period of one cell cycle. The temporal growth rate of each cell follows a Gaussian distribution. By solving the first time passage of the cell growth from $(2/3)n_0^{\text{cm}}$ to $(4/3)n_0^{\text{cm}}$, the mean and variance of the Gaussian distribution are uniquely determined, so cell cycle

periods can be distributed according to an inverse Gaussian distribution of mean $\tau_{\text{ave}}^{\text{cc}}$ and standard deviation $\tau_{\text{sd}}^{\text{cc}}$.

The potential energy function of the energy u_i^{cs} of the i^c th cell surface is given by

$$u_i^{\text{cs}} = \kappa^{\text{cs}} s_i^{\text{cs}}, \quad (9)$$

where the constant κ^{cs} is the cellular surface energy density.

3.2 Parameter settings

Supposing that the isolated single cells are in equilibrium, the force balances in the i^c th cell can be written from Eqs. (1) and (7) as follows.

$$\nabla_{j^v} u_{i^c}^{\text{cv}} + \nabla_{j^v} u_{i^c}^{\text{cs}} = \mathbf{0} \quad (10)$$

Then, substituting Eqs. (8) and (9) into Eq. (10), we obtain

$$\kappa^{\text{cs}} = n_{i^c}^{\text{cm}} k_B T \left(\frac{1}{v_{i^c}^{\text{cv}}} \right) \left(\frac{\partial v_{i^c}^{\text{cv}}}{\partial s_{i^c}^{\text{cs}}} \right). \quad (11)$$

Assuming that cells are spherical, their volume and surface area are related by

$$v_{i^c}^{\text{cv}} = \frac{(s_{i^c}^{\text{cs}})^{\frac{3}{2}}}{6\pi^{\frac{1}{2}}}, \quad (12)$$

from which Eq. (11) is rewritten as

$$\kappa^{\text{cs}} = \left(\frac{3}{32\pi} \right)^{\frac{1}{3}} n_{i^c}^{\text{cm}} k_B T (v_{i^c}^{\text{cv}})^{-\frac{2}{3}}. \quad (13)$$

Using the cell state with v_0^{cv} and n_0^{cm} as a standard, κ^{cs} is given by

$$\kappa^{\text{cs}} = \left(\frac{3}{32\pi} \right)^{\frac{1}{3}} n_0^{\text{cm}} k_B T (v_0^{\text{cv}})^{-\frac{2}{3}}. \quad (14)$$

Hence, κ^{cs} is expressed as a function of the other parameters.

To solve Eqs. (1) and (28), the parameter values were normalized by the unit length $l_0^c = (v_0^{\text{cv}})^{\frac{1}{3}}$, unit energy $n_0^{\text{cm}} k_B T$ and unit time $4\eta_0^{\text{ce}} (v_0^{\text{cv}})^{\frac{2}{3}} / n_0^{\text{cm}} k_B T$. Moreover, the unit stress, represented by σ_0 , is expressed by $n_0^{\text{cm}} k_B T / (v_0^{\text{cv}})^{\frac{1}{3}}$. All physical parameters are listed in Table 1.

Table 1 Physical parameters used in the model

Symbol	Value	Description	Related equation
$\eta_0^{\text{ee}} / \eta_0^{\text{ce}}$	0.0–10.0	Viscous friction weight of extracellular materials normalized by that of cells	(5)
$\tau_{\text{ave}}^{\text{cc}}$	2.0×10^2	Statistical average of cell cycle	(8)
$\tau_{\text{sd}}^{\text{cc}}$	5.0×10^{-4}	Variance of cell cycle	(8)

Assuming that cells are spherical, their volume and diameter are related by

$$v_0^{\text{cv}} = \frac{\pi (d_0^c)^3}{6}, \quad (15)$$

where d_0^c is the diameter of spherical cells. Using parameters κ^{cs} and d_0^c , units of length l_0^c and stress σ_0 can be rewritten as

$$l_0^c = \left(\frac{\pi}{6}\right)^{\frac{1}{3}} d_0^c, \quad (16)$$

and

$$\sigma_0 = 4 \frac{\kappa^{\text{cs}}}{d_0^c}, \quad (17)$$

respectively. For instance, endothelial cells whose diameter varies between 8 and 12 μm behave as a solid with a cortical tension of about 2,200 pN/ μm (Hochmuth 2000). In this case, the unit values of length l_0^c and stress σ_0 are estimated to be 6–10 μm and 700–1,100 pN/ μm^2 , respectively. Moreover, neutrophils with a diameter of about 8 μm behave as a liquid drop with a cortical tension of about 30 pN/ μm (Hochmuth 2000). In the case of cells with a property similar to neutrophils, the unit values of length l_0^c and stress σ_0 are estimated to be 6 μm and 15 pN/ μm^2 , respectively.

To focus on the effects of extracellular viscosity, the physical parameters of cell cycle, $\tau_{\text{ave}}^{\text{cc}}$ and $\tau_{\text{sd}}^{\text{cc}}$, are set to produce quasi-static processes in the case without extracellular viscosity ($\eta_0^{\text{ee}} = 0$). By comparing dimensions of the cellular surface tension κ^{cs} and viscous friction weight η_0^{ee} , the characteristic time of cell relaxation can be estimated to be of the order of $\eta_0^{\text{ee}}/\kappa^{\text{cs}}$. Hence, the cell cycle was set to be about 2.5×10^2 times larger than the characteristic time of cell relaxation. Hence, in simulations under the employed condition, cell deformations should immediately relax to be stable, so that each vertex velocity can be regarded as stationary at every moment. Therefore, the stress state of the entire tissue should relax to be approximately stress-free.

3.3 Results

To examine the advantage of the proposed model, simulation results of the proposed model were compared with those of a conventional model (setting $\mathbf{v}_i^f = \mathbf{0}$ in Eq. (1)). In addition, to demonstrate the applicability of the proposed model, the effects of the extracellular viscosity on epithelial morphologies were investigated. The parameter settings and numerical implementations are detailed in “Numerical implementation” section of “Appendix.”

3.3.1 Comparison of proposed and conventional models

In this investigation, the morphodynamics of directional epithelial growth were simulated in the absence of viscous

extracellular materials ($\eta_0^{\text{ee}} = 0$). The aim was to determine whether these models could produce stress-free vesicles in the global tissue scale, as expected under the employed condition for quasi-static processes.

Figure 3a plots the number of cells in an epithelial vesicle as a function of time t in both cases of the proposed and conventional models. The number of cells was an exponential function of time according to 2^t . Figure 3c–e shows the deformation processes of the epithelial vesicles simulated by the proposed and conventional models. The epithelial vesicles in the proposed model (Fig. 3c, d) were directly elongated in the growth direction, whereas those of the conventional model (Fig. 3c, e) were compactly undulated in the growth direction. These deformation processes are also shown in the Supplemental movie 1.

Figure 3f, g shows stress states of cells in the growth direction in epithelial vessels simulated by the proposed and conventional models, respectively. At the cell scale, various stresses appeared in the vessels simulated by both models, and the stress state in the conventional model tends to be more compressive than that in the proposed model. Figure 3b shows stress states of the entire tissue in the growth direction as a function of time. At the beginning of tissue growth, both models yielded nearly stress-free vessels. Even in the later period, stress remains nearly free in the vessels simulated by the proposed model, as expected in the absence of viscous extracellular materials. On the other hand, compressive stress appeared in the vessels simulated by the conventional model. Therefore, contrary to the expectation from the employed condition, the morphologies and stress states of the simulated epithelial vesicles drastically differed between the proposed and conventional models.

3.3.2 Effects of extracellular viscosity on epithelial morphodynamics

In this simulation, the viscous properties of extracellular materials η_0^{ee} were varied, and their effects on the morphology were examined. Figure 4a, b shows the global and local shapes of epithelial vesicles grown in materials with various viscosities. Oriented cell division deformed the epithelial vesicles into tubular shapes. At very low viscosity ($\eta_0^{\text{ee}}/\eta_0^{\text{ce}} = 10^{-4}$), the epithelial vesicle was linearly elongated, but tended to become buckled as the viscosity was raised. At intermediate viscosities ($\eta_0^{\text{ee}}/\eta_0^{\text{ce}} = 10^{-3}, 10^{-2}, 10^{-1}$), buckling was accompanied by branching. The branches tended to thicken as the viscosity increased. At high viscosity ($\eta_0^{\text{ee}}/\eta_0^{\text{ce}} = 10^0, 10^1$), the epithelial vesicles were both thickened and compactly undulated. Hence, the global and local shapes of epithelial vesicles were drastically altered by the extracellular viscosity. The deformation processes at inter-

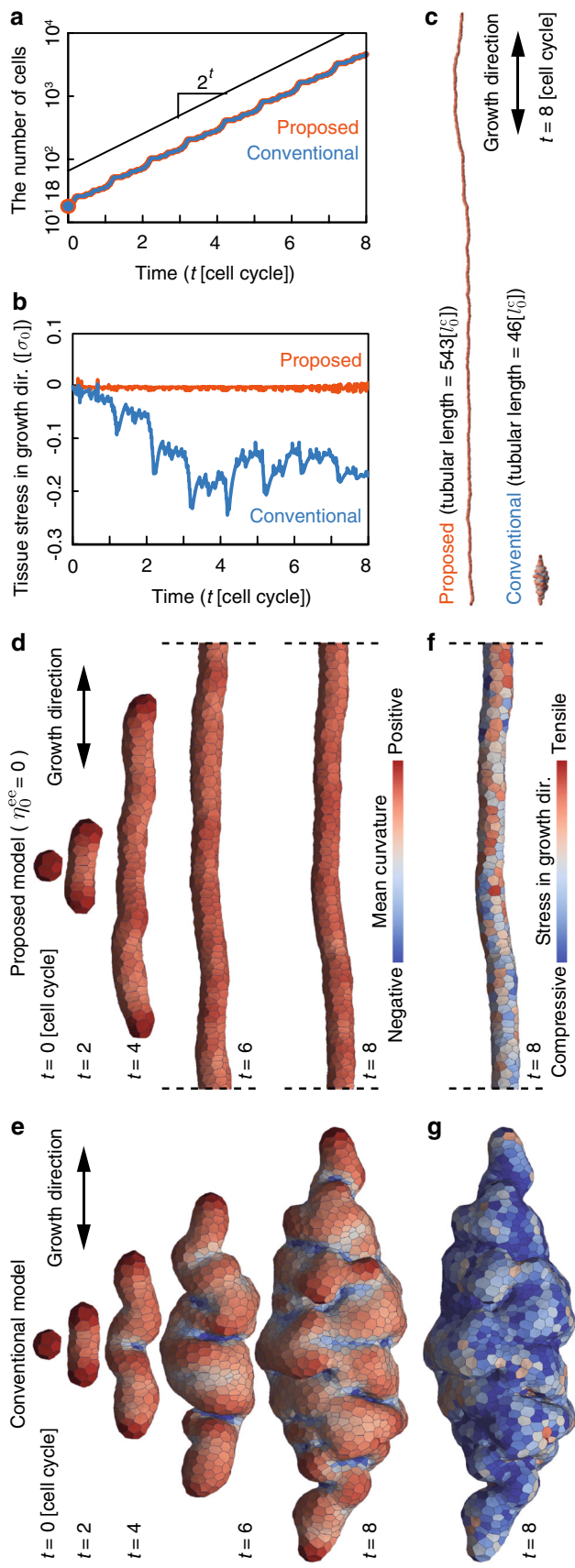


Fig. 3 Morphodynamics of directional epithelial growth. **a** The number of cells comprising an epithelial vesicle simulated by the proposed model (orange) and the conventional model (blue) as a function of time. The cell number grows as 2^t . **b** The overall stress of the epithelial vesicles simulated by the proposed model (orange) and the conventional model (blue) as a function of time. **c** The overall shapes of epithelial vesicles at $t = 8$ simulated by the proposed model (left) and the conventional model (right). **d**, **e** Time series images of growing epithelial vesicles at $t = 0, 2, 4, 6$ and 8 [cell cycles] simulated by the proposed and conventional models, respectively. Epithelial vesicles at $t = 6$ and 8 [cell cycles] simulated by the proposed model (d) are shown as being clipped at the dotted lines at its top and bottom. Colors indicate the local mean curvature of the individual epithelial vesicles. Cell stress of the epithelial vesicles simulated by the proposed model (f) and the conventional model (g) at $t = 8$ [cell cycles]

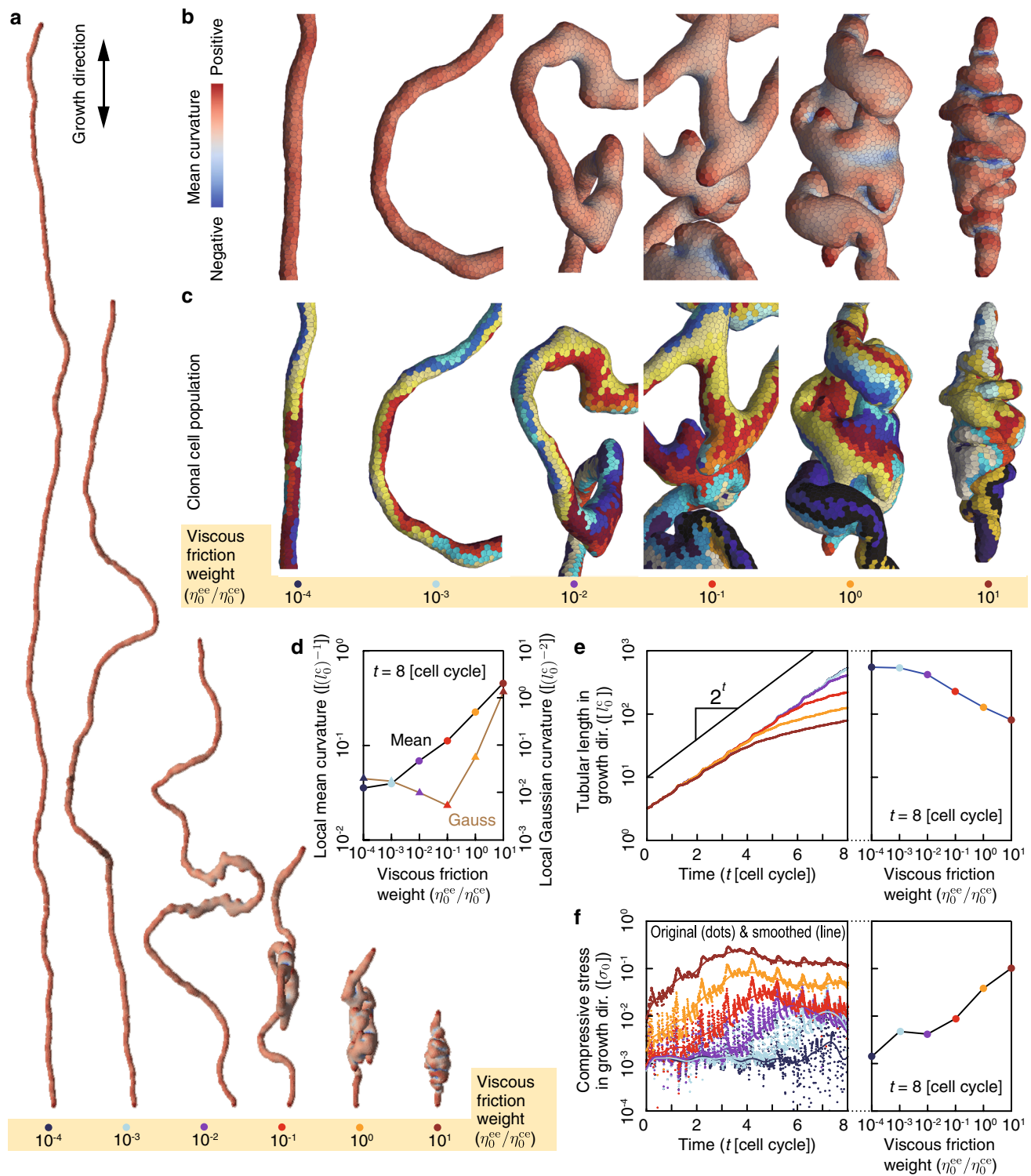


Fig. 4 Effects of extracellular viscosity on epithelial morphology. **a** Whole shapes of epithelial vesicles at different viscous friction weights ($\eta_0^{\text{ee}} / \eta_0^{\text{ce}} = 10^{-4}-10^1$) and $t = 8$ [cell cycles]. **b** Enlarged shapes of epithelial vesicles at viscous friction weights ($\eta_0^{\text{ee}} / \eta_0^{\text{ce}} = 10^{-4}-10^1$) and $t = 8$ [cell cycles]. The epithelial vesicle is colored by the local mean curvature. **c** Distributions of clonal cell populations in epithelial vesicles at different friction weights ($\eta_0^{\text{ee}} / \eta_0^{\text{ce}} = 10^{-4}-10^1$). Different colors indicate different clonal cell populations. **d** The spatial

average of the mean and Gaussian curvatures of local epithelial surfaces as functions of the viscous friction weight $\eta_0^{\text{ee}} / \eta_0^{\text{ce}}$. **e** Tubular length of epithelial vesicles in the growth direction as a function of time (left) and viscous friction weight (right). **f** Compressive force within the epithelial vesicles in the growth direction as a function of time (left) and viscous friction weight (right). Dots and line show original and smoothed data, respectively

mediate and high viscosities ($\eta_0^{\text{ee}}/\eta_0^{\text{ce}} = 10^{-2}, 10^{-1}, 10^0, 10^1$) are also shown in the Supplemental movie 2.

Figure 4c shows local shapes of epithelial vesicles, colored by clonal cell population. At low viscosity ($\eta_0^{\text{ee}}/\eta_0^{\text{ce}} = 10^{-4}, 10^{-3}$), clonal cells within the same population were distributed in a single line along the growth direction. As the viscosity was raised ($\eta_0^{\text{ee}}/\eta_0^{\text{ce}} = 10^{-2}, 10^{-1}, 10^0, 10^1$), cells from the same populations scattered both perpendicular to and along the growth direction. Because the perpendicular distribution of clonal cell populations increased the radius of the tubular epithelia, it thickened their tubular shapes. These results imply that the viscosity of the extracellular materials affects the cell configuration within tissue. The configurational dynamics of clonal cell populations at intermediate and high viscosities ($\eta_0^{\text{ee}}/\eta_0^{\text{ce}} = 10^{-2}, 10^{-1}, 10^0, 10^1$) are also shown in the Supplemental movie 4.

Figure 4d shows the spatial average of the mean and Gaussian curvatures of the local epithelial surfaces. The mean curvature remained positive but reduced with increasing viscosity. The Gaussian curvature was also positive, but minimized at intermediate viscosity ($\eta_0^{\text{ee}}/\eta_0^{\text{ce}} = 10^{-1}$). Physically, the epithelial surface turned more undulated at higher viscosities. Intermediate viscosities favored the development of saddle surfaces within branching structures. To quantify the viscous effects of the extracellular materials, several mechanical quantities were measured. Figure 4e shows the tubular lengths of epithelial vesicles in the growth direction. The tubular lengths were viscosity dependent and increased with time. At the lowest viscosity, the tubular length increased as 2^t . This phenomenon implies that the epithelial vesicles were elongated by cell proliferation while retaining their tubular radii. At higher viscosities, the tubular length saturates earlier, resulting in shorter vessels.

Figure 4f plots the stress states of the epithelial vesicles in the growth direction. Stress was estimated by the method described in the “Stress tensor estimation” section of “Appendix.” As the viscosity increased, stress turned more compressive, indicating the viscous frictions between the epithelial vesicle and extracellular materials to act on the epithelial vesicle. Therefore, the morphologies of the epithelial vesicles differed by the strength of the compressive forces imposed by the extracellular viscosity. Moreover, as shown in Fig. 4f, the apparent yield stress of epithelial vesicles are of the order of $10^{-2}\text{--}10^{-1} \sigma_0$. In the case of endothelial cells (Hochmuth 2000), the apparent yield stress is translated to be on the order of $10^1\text{--}10^2 \text{ pN}/\mu\text{m}^2$. Interestingly, this value is of the same order of the apparent stiffness of the overall Xenopus embryo during gastrulation (Davidson and Keller 2007; von Dassow and Davidson 2009). Furthermore, morphological changes in endothelial cells can be observed under shear stress on the order of $10^0\text{--}10^1 \text{ pN}/\mu\text{m}^2$ (Dewey et al. 1981).

4 Discussion

4.1 Proposed model reflecting timescale of tissue deformations

To examine the advantage of the proposed model, tissue morphodynamics were simulated without extracellular viscosity ($\eta_0^{\text{ee}} = 0$). In this condition, deformation processes can be regarded as quasi-static processes as described in Sect 3.2. From the proposed model, the epithelial vesicles grew into a straight elongated structure with a nearly stress-free state in the global tissue scale (Fig. 3d, b). The nearly free stress corresponds to the employed condition for quasi-static processes. In contrast, the conventional model yielded thick, undulated epithelial vessels (Fig. 3e). Remarkably, although extracellular viscosity is not considered in the conventional model, the epithelial vesicle became highly compressed in the global tissue scale, as shown in Fig. 3b. The high residual stress conflicts with the employed condition for quasi-static processes. Because the compressive forces oppose the direction of epithelial growth, they appear to be viscous resistance forces resulting from the violation of Galilean invariance (see “Galilean invariance of vertex dynamics model” section of “Appendix”). Therefore, the differences in these morphologies and stress states reflect the question of whether the model satisfied the Galilean invariance.

By setting the growth rate much lower than the viscous relaxation of cell deformations, conventional models can also produce straight tubular morphologies similar to that of the proposed model. This is because tissue deformations approach quasi-static processes with decreasing growth rate. Supposing quasi-static deformation processes, the effects of the viscous force term in Eq. (28) can be ignored. Hence, the conventional model can be approximated to satisfy Galilean invariance as well as the proposed model. However, in terms of the timescale of deformation processes, tissue deformations should be regarded as quasi-static deformation processes as described in Sect. 3.2. Therefore, the timescale of tissue deformations cannot be taken into account in the conventional model. These results suggest that the proposed model overcomes this problem by satisfying Galilean invariance. Therefore, from a mechanical viewpoint, the timescale of tissue deformations is qualitatively reflected in the proposed model.

Interestingly, the epithelial shape yielded by the conventional model (Fig. 3e) is very similar to that yielded by the proposed model with high extracellular viscosity ($\eta_0^{\text{ee}}/\eta_0^{\text{ce}} = 10^1$) (Fig. 4c). This implies that viscous resistance forces resulting from the violation of Galilean invariance play a similar role to those resulting from extracellular viscosities. However, the proposed and conventional models primarily express diverse physical phenomena. From the viewpoint of soft matter physics, while conventional models employing

Eq. (28) express the movement of particles in a stationary dilute liquid, the proposed model employing Eq. (1) express the movement of a condensed matter. Moreover, by introducing Eqs. (2), (3) and (4), the proposed model enables the expression of the inner structure of the condensed matter as the viscous effects of tissue components.

4.2 Dynamic tissue deformations depending on extracellular viscosity

To examine the applicability of the proposed model, the extracellular viscosity was varied, and its effects on epithelial morphodynamics were analyzed. In the simulations using the proposed model, epithelial vesicle deformations were highly sensitive to extracellular viscosity (see Fig. 4a–e). These deformations are quantified by the mean and Gaussian curvatures, as shown in Fig. 4d. The different deformations stemmed from the different strengths of the compressive forces generated by viscous frictions between the epithelial cells and extracellular materials (Fig. 4f). The strength of the compressive force governed the bending, branching and thickening of the tubular epithelia (Fig. 4a). Moreover, it is physically reasonable that the compressive forces increased with time. This is because viscous resistance forces increase linearly to the growth rate of tubular lengths. Furthermore, higher compressive forces likely show higher apparent yield points and encourage the bending and thickening of tubular epithelia at higher extracellular viscosities. Therefore, the proposed model can express dynamic processes of various tissue deformations depending on the extracellular viscosity. Because the apparent yield stress observed in the simulations have admissible values, from a mechanical viewpoint, the predicted effects of extracellular viscosity could be possibly involved in real processes of tissue morphogenesis.

The branching shapes observed at intermediate viscosities appear to develop by epithelial growth from the bent area of the epithelial vesicle. The thickening of the tubular epithelia at high viscosities seems to be attributed to cell rearrangements, which are driven by stronger compressive forces than those required for bending. In the simulations, the directions of cell divisions are oriented along the global axis of the growth direction. In the manner of division, divided cells are linearly aligned in the growth direction. Hence, the tubular epithelia tend to elongate linearly along the growth direction. At low viscosity, the tubular epithelia tend to grow linearly along the growth direction under low viscous resistance forces. Hence, divided cells tend to remain aligned in the growth direction. On the other hand, at high viscosity, the tubular epithelia tend to buckle under the increasing viscous resistance forces, and the axial directions of tubes tend to deviate from the growth direction. Simultaneously, the linearly aligned, divided cells also deviate from the growth direction. Therefore, at high viscosity, the clonal cells tend

to scatter not only along but also perpendicular to the growth direction.

4.3 Applicability and future perspectives

The proposed model successfully simulated viscosity-dependent dynamic deformation processes. Because the proposed model is constructed on a general framework of viscous properties, it can express the viscous properties of different tissue components such as cytoplasm, cytoskeleton, basement membrane and ECM. These viscous properties are expressed by modifying the viscous friction and local velocity functions [Eqs. (5) and (6), respectively]. Moreover, the proposed model can be applied to simulating tissue morphodynamics with flows of tissue components. Although extracellular materials are supposed to be stationary for simplification in the simulations, morphodynamics driven by surrounding tissues could also be important in tissue morphogenesis. For instance, extrinsic forces can come from flows of fluids at the surface of tissues (Hahn et al. 2009; Lye and Sanson 2011). Furthermore, shear stress generated by fluid flows could affect the morphologies and functions of endothelial cells covering the inner surface of vascular wall (Dewey et al. 1981). Such effects of flows could also be applicable targets of simulations using the proposed model. Combining the proposed model with the immersed boundary method (Mittal and Iaccarino 2005) is another significant idea for expressing mechanical interactions between tissue deformations and fluid flows. Therefore, the proposed model is recommended as a useful multicellular dynamics approach for analyzing the viscous effects of various tissue components on tissue deformation.

A current challenge in the developmental biology is to understand how tissue morphogenesis emerges from molecular interactions in a biochemical regulatory background. The mechanics of tissue morphogenesis are complicated by the spatiotemporal scale gap from molecules to tissues. The proposed model may assist in elucidating the underlying mechanical phenomena from the sub-cellular to the multicellular scale. Thus, the proposed model provides an approach for multi-scale simulations, which will contribute to linking cell biology and developmental biology as well as to understanding the biomechanics of developmental morphogenesis.

5 Conclusion

This study has presented a vortex dynamics model for simulating viscosity-dependent dynamic deformation processes during tissue morphogenesis. Local velocity fields were included in the governing equation of vertex movements. These local fields ensured that the Galilean invariance was satisfied in the model. In addition, the viscous properties of

tissue components were newly expressed by formulating the friction forces on vertices as functions of the relative velocities among the vertices. The advantage and applicability of the proposed model was assessed in the dynamic deformation simulations of directional epithelial growth. Under the employed condition for quasi-static processes, the morphologies and stress states of epithelial vesicles drastically differed between the proposed and conventional models, where straight tubes with nearly free stress were obtained by the proposed model, and thick, undulated tubes with compressive residual stress were obtained by the conventional model. These results suggest that the proposed model is able to reflect the timescale of tissue deformations because it satisfies Galilean invariance. When the epithelial vesicles were surrounded by viscous extracellular materials, they deformed by oriented cell divisions and their morphologies were highly sensitive to extracellular viscosity. In particular, low viscosity yielded straight tubes, intermediate viscosities yielded undulated tubes with buckling as well as branching and high viscosities resulted in thickened, undulated tubes. Thus, the proposed model successfully captures the viscosity-dependent dynamic deformation processes during tissue morphogenesis.

Acknowledgments The authors appreciate valuable comments from Dr. Yoshihiro Morishita, Katsuhiko Sato and Yukitaka Ishimoto at the RIKEN Center for Developmental Biology, Japan. This study was supported by JSPS KAKENHI Grant Numbers 25889070.

Appendix

Balance of friction forces among the vertices of a geometrical element

Friction forces are exerted between multiple bodies moving at different velocities. In the proposed model, viscous frictions are defined at the several vertices comprising each geometrical element.

From Eq. (4), the viscous friction force exerted on the i^v th vertex, represented by $f_{i^v}^v$, is given by

$$f_{i^v}^v = \sum_{j^e}^{\text{element}} \eta_{j^e}^v (\mathbf{v}_{i^v} - \mathbf{v}_{j^e}) \delta_{i^v; j^e} \quad (18)$$

$$= \sum_{j^e}^{\text{element}} \eta_{j^e}^v \left(\mathbf{v}_{i^v} - \frac{1}{n_{j^e}^v} \sum_{k^v}^{\text{vertex}} \mathbf{v}_{k^v} \delta_{k^v; j^e} \right) \delta_{i^v; j^e} \quad (19)$$

$$= \sum_{k^v}^{\text{vertex}} \sum_{j^e}^{\text{element}} \frac{\eta_{j^e}^v}{n_{j^e}^v} \delta_{k^v; j^e} \delta_{i^v; j^e} (\mathbf{v}_{i^v} - \mathbf{v}_{k^v}), \quad (20)$$

where \mathbf{v}_{i^v} is the displacement velocity of the i^v th vertex, $d\mathbf{r}_{i^v}/dt$.

To derive the viscous friction force exerted on the i^v th vertex by the l^v th vertex, Eq. (20) is multiplied by the following equation.

$$1 = \delta_{k^v l^v} + (1 - \delta_{k^v l^v}), \quad (21)$$

where $\delta_{k^v l^v}$ is the Kronecker delta function. The force $f_{i^v}^v$ can now be separated into two forces in terms of $k^v = l^v$ and $k^v \neq l^v$ as follows.

$$\begin{aligned} f_{i^v}^v &= \sum_{k^v}^{\text{vertex element}} \sum_{j^e}^{\text{element}} \frac{\eta_{j^e}^v}{n_{j^e}^v} \delta_{k^v; j^e} \delta_{i^v; j^e} (\mathbf{v}_{i^v} - \mathbf{v}_{k^v}) \delta_{k^v l^v} \\ &+ \sum_{k^v}^{\text{vertex element}} \sum_{j^e}^{\text{element}} \frac{\eta_{j^e}^v}{n_{j^e}^v} \delta_{k^v; j^e} \delta_{i^v; j^e} (\mathbf{v}_{i^v} - \mathbf{v}_{k^v}) (1 - \delta_{k^v l^v}). \end{aligned} \quad (22)$$

Hence, the viscous friction force $f_{i^v l^v}^{vv}$, exerted on the i^v th vertex by the l^v th vertex, is the first term involving $\delta_{k^v l^v}$ in Eq. (22):

$$f_{i^v l^v}^{vv} = \sum_{j^e}^{\text{element}} \frac{\eta_{j^e}^v}{n_{j^e}^v} \delta_{i^v; j^e} \delta_{l^v; j^e} (\mathbf{v}_{i^v} - \mathbf{v}_{l^v}). \quad (23)$$

According to Eq. (23), $f_{i^v l^v}^{vv}$ is a linear function of the relative velocity. Therefore, the viscous friction coefficient of the i^v th vertex introduced by the l^v th vertex given by $\eta_{i^v l^v}^{vv}$ can be written as

$$\eta_{i^v l^v}^{vv} = \sum_{j^e}^{\text{element}} \frac{\eta_{j^e}^v}{n_{j^e}^v} \delta_{i^v; j^e} \delta_{l^v; j^e}. \quad (24)$$

The viscous friction coefficients between the i^v th and the l^v th vertices are then related by

$$\eta_{i^v l^v}^{vv} = \eta_{l^v i^v}^{vv}. \quad (25)$$

Thus, the viscous friction coefficients are symmetric for any pair of vertices.

Using Eq. (23), the sum of viscous friction forces between a pair of vertices is given by

$$f_{i^v l^v}^{vv} + f_{l^v i^v}^{vv} = \mathbf{0}. \quad (26)$$

Thus, the viscous friction forces exerted between any two vertices are balanced.

Galilean invariance of vertex dynamics model

The following theoretical analysis clarifies whether the vertex dynamics in the proposed and conventional models are invariant under the Galilean transformation. The Galilean transformation is

$$\tilde{\mathbf{r}}_{i^v} = \mathbf{r}_{i^v} + \mathbf{V}t, \quad (27)$$

where \mathbf{V} is an arbitrary velocity vector. Substituting Eq. (27) in Eq. (1), we retrieve Eq. (1). Hence, the proposed model is invariant under the Galilean transformation.

The conventional models (Honda et al. 2004; Okuda et al. 2013a,b,c) neglect the local velocity vectors (i.e., $\mathbf{v}_i^f = \mathbf{0}$ in Eq. (1)). Hence, the movement of the i^v th vertex is given by

$$\eta_i^v \frac{d\mathbf{r}_{i^v}}{dt} = -\nabla_{i^v} U. \quad (28)$$

Substituting Eq. (27) into Eq. (28), we obtain

$$\eta_i^v \frac{d\tilde{\mathbf{r}}_{i^v}}{dt} = -\nabla_{i^v} U - \eta_0^v \mathbf{V}. \quad (29)$$

Compared to Eq. (29), Eq. (28) contains an additional force term $-\eta_0^v \mathbf{V}$. Thus, the conventional models described by Eq. (28) violate Galilean invariance unless the additional force can be ignored.

Cell rearrangement and division behaviors

Cell rearrangement is expressed by reconnecting local network patterns using the reversible network reconnection (RNR) model (Okuda et al. 2013a). The RNR model generates continuous cell rearrangements that are geometrically, energetically and topologically reversible. Cell proliferation is accomplished by a cell proliferation model (Okuda et al. 2013b), in which cells divide (increase their number) and grow (increase their volume). In particular, cell division is simulated by dividing a single polyhedron along a plane.

When the number of molecules in the i^c th cell $n_{i^c}^{cm}$ increases to $(4/3)n_0^{cm}$, the i^c th cell divides into two daughter cells. The dividing plane is regulated to be normal to the plane of the cell sheet and globally oriented along the growth direction, as shown in Fig. 2a. The normal direction of the cell plane is specified as a vector pointing from the center of an outside polygonal face of each cell to the center of that cell. Details of the cell division are similar to those of the global regulation used in our previous study (Okuda et al. 2013c).

Numerical implementation

Equations (1) and (28) were numerically time-integrated using the Euler method with a time step of Δt . Vertex velocities in Eq. (1) were iteratively solved by convergent calculations. Convergence was reached when the mean residual error was below the threshold RE_{th} , as follows.

$$\left| \eta_i^v \left(\frac{d\mathbf{r}_{i^v}}{dt} - \mathbf{v}_{i^v}^f \right) + \nabla_{i^v} U \right| \leq RE_{th} \quad (30)$$

Local network patterns were reconnected when each edge included in a local pattern turned shorter than a specified threshold Δl_{th} . The reconnection rule was trialed at each

Table 2 Numerical parameters used in the model

Symbol	Value	Description	Related equation
Δt	5.0×10^{-3}	Integration time step	(1)
RE_{th}	1.0×10^{-5}	Threshold for residual error	(1)
Δt_r	1.0	Time interval of network reconnections	—
Δl_{th}	5.0×10^{-2}	Threshold length of network reconnections	—

edge and each trigonal face during each time interval Δt_r . Numerical parameters are listed in Table 2.

All experiments were performed on a cluster computer comprising 12 nodes with 2.9 GHz Intel Xeon dual processors and 64 GB RAM (Visual Technology Co., Japan).

Stress tensor estimation

To analyze the deformation mechanics within the tissues, stress tensors were estimated from the locations and forces of vertices according to (Hardy 1982).

The stress tensor σ_v over the whole epithelial vesicle is estimated as

$$\sigma_v = -\frac{1}{v_t} \sum_{j^v}^{\text{vertex}} \left(\mathbf{r}_{j^v} \otimes \frac{\partial U}{\partial \mathbf{r}_{j^v}} \right), \quad (31)$$

where the scalar v_t is the volume of the epithelial vesicle, and $\sum_{j^v}^{\text{vertex}}$ denotes the summation overall vertices. The stress tensor σ_{i^c} at the i^c th cell is estimated as

$$\sigma_{i^c} = -\frac{1}{v_{i^c}} \sum_{j^v}^{\text{vertex}} \left(\mathbf{r}_{j^v} \otimes \mathbf{f}_{i^c j^v}^{cv} \right) \delta_{j^v; i^c}, \quad (32)$$

where the scalar v_{i^c} is the volume of the i^c th cell, and $\sum_{j^v}^{\text{vertex}}$ sums overall vertices. Vector $\mathbf{f}_{i^c j^v}^{cv}$ denotes the interior force of the i^c th cell exerted on the j^v th vertex:

$$\mathbf{f}_{i^c j^v}^{cv} = -\nabla_{j^v} (u_{i^c}^{cv} + u_{i^c}^{cs}). \quad (33)$$

References

- Borghi N, James Nelson W (2009) Intercellular adhesion in morphogenesis: molecular and biophysical considerations. Curr Top Dev Biol 89:1–32
- Brochard-Wyart F, de Gennes P-G (2003) Unbinding of adhesive vesicles. Comptes Rendus Phys 4:281–287
- Cuvelier D, Theory M, Chu YS, Dufour S, Theory JP, Bornens M, Nasso P, Mahadevan L (2007) The universal dynamics of cell spreading. Curr Biol 17:694–699
- Dahmann C, Oates AC, Brand M (2011) Boundary formation and maintenance in tissue development. Nat Rev Genet 12(1):43–55

- Davies JA (2005) Mechanisms of morphogenesis: the creation of biological form. Elsevier, Burlington
- Davidson L, Keller R (2007) Measuring mechanical properties of embryos and embryonic tissues. *Methods Cell Biol* 83:425–439
- Dewey CF Jr, Bussolari SR, Gimbrone MA Jr, Davies PF (1981) The dynamic response of vascular endothelial cells to fluid shear stress. *J Biomech Eng* 103(3):177–185
- Eiraku M, Takata N, Ishibashi H, Kawada M, Sakakura E, Okuda S, Sekiguchi K, Adachi T, Sasai Y (2011) Self-organizing optic-cup morphogenesis in three-dimensional culture. *Nature* 472(7341):51–56
- Farhadifar R, Röper JC, Aigouy B, Eaton S, Jülicher F (2007) The influence of cell mechanics, cell-cell interactions, and proliferation on epithelial packing. *Curr Biol* 17(24):2095–2104
- Goldstein H, Poole CP, Safko JL (2000) Classical Mechanics, 3rd edn. Addison-Wesley, Boston
- Hahn C, Schwartz MA (2009) Mechanotransduction in vascular physiology and atherogenesis. *Nat Rev Mol Cell Biol* 10(1):53–62
- Hardy RJ (1982) Formulas for determining local properties in molecular-dynamics simulations: Shock waves. *J Chem Phys* 76(1):622–628
- He B, Doubrovinski K, Polyakov O, Wieschaus E (2014) Apical constriction drives tissue-scale hydrodynamic flow to mediate cell elongation. *Nature*. doi:10.1038/nature13070
- Heisenberg CP, Tada M, Rauch GJ, Saúde L, Concha ML, Geisler R, Stemple DL, Smith JC, Wilson SW (2000) Silberblick/Wnt11 mediates convergent extension movements during zebrafish gastrulation. *Nature* 405:76–81
- Hochmuth RM (2000) Micropipette aspiration of living cells. *J Biomech* 33(1):15–22
- Honda H, Yamanaka H (1984) A computer simulation of geometrical configurations during cell division. *J Theor Biol* 106(3):423–435
- Honda H, Nagai T, Tanemura M (2008) Two different mechanisms of planar cell intercalation leading to tissue elongation. *Dev Dyn* 237(7):1826–1836
- Honda H, Tanemura M, Nagai T (2004) A three-dimensional vertex dynamics cell model of space-filling polyhedra simulating cell behavior in a cell aggregate. *J Theor Biol* 226(4):439–453
- Ishimoto Y, Morishita Y (submitted) Bubbly vertex dynamics: a dynamical and geometrical model for epithelial tissues with curved cell shapes. arXiv:1405.3839
- Lecuit T, Lenne PF (2007) Cell surface mechanics and the control of cell shape, tissue patterns and morphogenesis. *Nat Rev Mol Cell Biol* 8(8):633–644
- Rauzi M, Lenne PF, Lecuit T (2010) Planar polarized actomyosin contractile flows control epithelial junction remodeling. *Nature* 468(7327):1110–1114
- Letizia A, Sotillos S, Campuzano S, Llimargas M (2011) Regulated Crb accumulation controls apical constriction and invagination in Drosophila tracheal cells. *J Cell Sci* 124(2):240–251
- Lye CM, Sanson B (2011) Tension and epithelial morphogenesis in Drosophila early embryos. *Curr Top Dev Biol* 95:145–187
- Mao Y, Tournier AL, Hoppe A, Kester L, Thompson BJ, Tapon N (2013) Differential proliferation rates generate patterns of mechanical tension that orient tissue growth. *EMBO J* 32(21):2790–2803
- Metzger RJ, Klein OD, Martin GR, Krasnow MA (2008) The branching programme of mouse lung development. *Nature* 453(7196):745–750
- Mittal R and Iaccarino G (2005) Immersed boundary methods. *Annu Rev Fluid Mech* 37:239–261
- Odell GM, Oster G, Alberch P, Burnside B (1981) The mechanical basis of morphogenesis. 1. Epithelial folding and invagination. *Dev Biol* 85(2):446–462
- Okuda S, Inoue Y, Eiraku M, Sasai Y, Adachi T (2013a) Reversible network reconnection model for simulating large deformation in dynamic tissue morphogenesis. *Biomech Model Mechanobiol* 12(4):627–644
- Okuda S, Inoue Y, Eiraku M, Sasai Y, Adachi T (2013b) Modeling cell proliferation for simulating three-dimensional tissue morphogenesis based on a reversible network reconnection framework. *Biomech Model Mechanobiol* 12(5):987–996
- Okuda S, Inoue Y, Eiraku M, Sasai Y, Adachi T (2013c) Apical contractility in growing epithelium supports robust maintenance of smooth curvatures against cell-division-induced mechanical disturbance. *J Biomech* 46(10):1705–1713
- Osterfield M, Du X, Schüpbach T, Wieschaus E, Shvartsman SY (2013) Three-dimensional epithelial morphogenesis in the developing Drosophila egg. *Dev Cell* 24(4):400–410
- Rauzi M, Verant P, Lecuit T, Lenne PF (2008) Nature and anisotropy of cortical forces orienting Drosophila tissue morphogenesis. *Nat Cell Biol* 10(12):1401–1410
- Taniguchi K, Maeda R, Ando T, Okumura T, Nakazawa N, Hatori R, Nakamura M, Hozumi S, Fujiwara H, Matsuno K (2011) Chirality in planar cell shape contributes to left-right asymmetric epithelial morphogenesis. *Science* 333(6040):339–341
- Unterberger MJ, Schmoller KM, Wurm C, Bausch AR, Holzapfel GA (2013) Viscoelasticity of cross-linked actin networks: experimental tests, mechanical modeling and finite-element analysis. *Acta Biomater* 9(7):7343–7353
- Park S, Koch D, Cardenas R, Käs J, Shih CK (2005) Cell motility and local viscoelasticity of fibroblasts. *Biophys J* 89(6):4330–4342
- von Dassow M, Davidson LA (2009) Natural variation in embryo mechanics: gastrulation in *Xenopus laevis* is highly robust to variation in tissue stiffness. *Dev Dyn* 238(1):2–18
- Woolner S, Papalopulu N (2012) Spindle position in symmetric cell divisions during epiboly is controlled by opposing and dynamic apicobasal forces. *Dev Cell* 22(4):775–787